Earth and Planetary Science Letters 306 (2011) 137–148

Contents lists available at ScienceDirect

Earth and Planetary Science Letters

journal homepage: www.elsevier.com/locate/epsl

Towards quantitative sea ice reconstructions in the northern North Atlantic: A combined biomarker and numerical modelling approach

Juliane Müller [a,*], Axel Wagner [a,b], Kirsten Fahl [a], Ruediger Stein [a], Matthias Prange [b,c], Gerrit Lohmann [a,b]

[a] Alfred Wegener Institute for Polar and Marine Research, Bremerhaven, Germany
[b] University of Bremen, Germany
[c] MARUM, Center for Marine Environmental Sciences, Bremen, Germany

ARTICLE INFO

Article history:
Received 24 November 2010
Received in revised form 4 April 2011
Accepted 14 April 2011
Available online 2 May 2011

Editor: P. DeMenocal

Keywords:
Northern North Atlantic
sea ice
biomarkers
IP_{25}
Ocean–sea ice model

ABSTRACT

Organic geochemical analyses of marine surface sediments from the continental margins of East Greenland and West Spitsbergen provide for a biomarker-based estimate of recent sea ice conditions in the northern North Atlantic. By means of the sea ice proxy IP_{25} and phytoplankton derived biomarkers (e.g. brassicasterol and dinosterol) we reconstruct sea ice and sea surface conditions, respectively. The combination of IP_{25} with a phytoplankton marker (in terms of a phytoplankton marker-IP_{25} index; PIP_{25}) proves highly valuable to properly interpret the sea ice proxy signal as an under- or overestimation of sea ice coverage can be circumvented. A comparison of this biomarker-based assessment of the sea ice distribution in the study area with (1) modern remote sensing data and (2) numerical modelling results reveal a good agreement between organic geochemical, satellite and modelling observations. The reasonable simulation of modern sea ice conditions by means of a regional ocean–sea ice model demonstrates the feasibility to effectively integrate the complex atmospheric and oceanic circulation features as they prevail in the study area. The good correlation between modelled sea ice parameters and the biomarker-based estimate of sea ice coverage substantiates that linking proxy and model data occurs to be a promising concept in terms of a cross-evaluation. This combinatory approach may provide a first step towards quantitative sea ice reconstructions by means of IP_{25}. Future IP_{25} studies on marine surface sediments from the Arctic realm, however, are recommended to extend and validate this new attempt of using IP_{25} in combination with a phytoplankton marker as a quantitative measure for sea ice reconstructions.

1. Introduction

Arctic sea ice is a pivotal element of the global climate as it influences the heat and moisture exchange between the ocean and the atmosphere. Furthermore it significantly affects the oceanic heat transfer and salinity regulation between southern and northern latitudes, thus impacting on the thermohaline circulation in the northern North Atlantic (e.g. Dieckmann and Hellmer, 2003; Rudels, 1996).

Information on modern Arctic sea ice conditions derive mainly from remote sensing data (e.g. Gloersen et al., 1992; Spreen et al., 2008) and research vessel observations (for instance, sediment trap and buoy data; e.g. Bauerfeind et al., 2005; Fahl and Nöthig, 2007; Perovich et al., 2009; see Eicken et al., 2009 for further field techniques) and allow for the monitoring of the most recent development of sea ice coverage in higher latitudes. Besides the concern about its future development, the currently observed retreat of Arctic sea ice, however, also prompts a gaining interest in past (natural) variations of the sea ice extent in the Arctic Ocean.

Most studies on the palaeodistribution of sea ice are commonly based on sedimentological data (Knies et al., 2001; Spielhagen et al., 2004) and microfossils (e.g. Carstens and Wefer, 1992; Koç et al., 1993; Matthiessen et al., 2001; Polyak et al., 2010; for a recent review see Stein, 2008). In particular, sea ice associated (sympagic) organisms (e.g. pennate ice diatoms; Horner, 1985) which contribute remarkably to the primary production in the marine Arctic ice environment (Gosselin et al., 1997; Gradinger, 2009), are frequently used for reconstructing sea ice conditions (Abelmann, 1992; Justwan and Koç, 2008; Koç et al., 1993; Kohly, 1998). However, it has also been shown previously that the preservation of fragile siliceous diatom frustules can be relatively poor in surface sediments from the Arctic realm and the same is also true (if not worse) for calcareous-walled microfossils, thus limiting their application potential (Kohly, 1998; Matthiessen et al., 2001; Schlüter and Sauter, 2000; Steinsund and Hald, 1994).

In recent decades, the organic geochemical investigation of marine sediments for specific molecular tracers (biomarkers), which are indicative of the type of organic matter they are derived from, has

* Corresponding author.
E-mail address: juliane.mueller@awi.de (J. Müller).

0012-821X/$ – see front matter © 2011 Elsevier B.V. All rights reserved.
doi:10.1016/j.epsl.2011.04.011

become a valuable tool for assessing palaeoenvironmental conditions (e.g. Eglinton and Eglinton, 2008; Meyers, 1997; Stein and Macdonald, 2004; Volkman, 2006). The novel sea ice proxy IP_{25} (Belt et al., 2007), a monounsaturated highly branched isoprenoid lipid associated with diatoms that are restricted to sea ice, has been successfully used as a direct proxy for sea ice coverage. The identification of this molecule in marine sediment cores from the Canadian Arctic Archipelago, the shelf north off Iceland and from northern Fram Strait, thus enabled reconstructions of the ancient sea ice variability in these regions (Belt et al., 2010; Massé et al., 2008; Müller et al., 2009; Vare et al., 2009). We recently demonstrated that the additional use of the phytoplankton-derived biomarker brassicasterol (e.g. Goad and Withers, 1982; Kanazawa et al., 1971; Volkman, 2006) as an indicator for open-water conditions notably facilitates the environmental reconstruction as ambiguous IP_{25} signals (i.e. its absence, which may refer to either a lack of sea ice or, in contrast, a permanent and thick ice cover limiting any algal growth) can be circumvented (Müller et al., 2009).

Along with these proxy-based sea ice reconstructions, physically based numerical ocean–sea ice models provide a complementary tool as they consider thermodynamic and dynamic key elements that shape sea surface and sea ice conditions. A particularly beneficial feature of these models is the possibility to reproduce sea ice thickness. The instrumental assessment of ice thickness (e.g. by means of ice-floe drilling, upward-looking sonar, ground-based/airborne EM; see Haas and Druckenmiller, 2009 for review) is still a spatially limited method, especially when compared to the relatively straightforward determination of the extent or concentration of sea ice by remote sensing. Ocean–sea ice models therefore provide a valuable source of ice thickness estimates that may be potentially useful within palaeo sea ice studies. However, the assessment of a model's accuracy (in representing sea ice conditions) reasonably builds on comparisons with observational (mainly satellite) or proxy data. With particular regard to palaeo-modelling studies, a calibration of proxy- and model-based assumptions of sea ice conditions would certainly improve forthcoming climate/sea ice reconstructions.

As the major discharge of Arctic sea ice to the northern North Atlantic occurs through Fram Strait (Fig. 1; Aagaard and Coachman, 1968; Rudels et al., 2005) marine sediments from this region may serve as ideal climate archives and provide useful information about the dynamics of this sea ice export system. With the organic geochemical analyses of surface sediments from the continental margins of East Greenland and West Spitsbergen, we herein give insight into the modern environmental situation of these areas. In addition to relatively common phytoplankton derived biomarkers (short-chain *n*-alkanes, certain sterols) we mainly focus on the sea ice proxy IP_{25} to estimate (spring/summer) sea ice conditions and to evaluate the applicability of this relatively novel ice proxy in an area of highly variable (seasonal) ice cover and strong ocean surface currents. With the incorporation of numerically modelled modern (spring) sea ice concentrations and thicknesses, we finally aim at a cross-evaluation of proxy and model data, which may give direction towards a quantitative assessment of sea ice conditions in the past with implications for predictions of the future.

2. Regional setting

The oceanographic setting in Fram Strait is characterised by two opposing current systems separating the passage into a comparatively temperate eastern region and a polar western domain. Warm Atlantic water enters the Nordic Seas via the northward heading Norwegian Current (NC) and, to a minor extent, via the Irminger Current (IC) west of Iceland (Fig. 1; after Rudels et al., 2005). In eastern Fram Strait the warm Atlantic water enters the Arctic Ocean via the West Spitsbergen Current (WSC). In western Fram Strait, polar water from the Arctic Ocean is transported southwards by the East Greenland Current (EGC) along the East Greenland continental margin (Aagaard and Coachman, 1968). Sea ice conditions in the study area are hence subjected to (1) a massive seasonal discharge of old/multi-year sea ice and icebergs via the EGC and (2) the formation of new sea ice during autumn and winter. In general, the ice cover is more extensive in duration and concentration in coastal and proximal shelf areas of the East Greenland continental margin with a pronounced southward sea-ice drift parallel to the coast (e.g. Gloersen et al., 1992; Martin and Wadhams, 1999). A frequent and prominent winter sea ice feature is the development of the Odden ice tongue (lasting until early spring), which covers the catchment area of the cold Jan Mayen Current in the central Greenland Sea (72°–74°N; Fig. 1; Comiso et al., 2001; Wadhams et al., 1996).

As the WSC supplies eastern Fram Strait with warm Atlantic water, sea ice conditions at the West Spitsbergen continental margin are less severe. Winter sea ice formation is confined largely to near-shore areas and the fjords with the latter remaining covered in fast ice until early summer (Wiktor, 1999). Furthermore, ice conditions are subjected to the northward advection of sea ice that originates from the Barents Sea (Boyd and D'Asaro, 1994; Haugan, 1999).

3. Materials and methods

3.1. Sediment samples and geochemical treatment

The surface sediment samples (0–1 cm; n = 44) studied herein were obtained during RV Polarstern cruises ARK-X/2 (Hubberten, 1995), ARK-XVI/1-2 (Krause and Schauer, 2001), ARK-XVIII/1 (Lemke, 2003) and ARK-XIX/4 (Jokat, 2004) by means of box- and multicoring equipment. Sediments were collected along the East Greenland continental margin (including the continental slope and adjacent deep-sea) and the continental margin of West Spitsbergen (Fig. 1; see Table 1 for coordinates of sampling locations). All samples were stored in clean brown glass vials at −30 °C until further treatment. For lipid biomarker analyses, the freeze-dried and homogenised sediments were extracted with an Accelerated Solvent Extractor (DIONEX, ASE 200; 100 °C, 5 min, 1000 psi) using a dichloromethane: methanol mixture (2:1 v/v). Prior to this step, 7-hexylnonadecane (0.1064 μg/sample), squalane (0.6 μg/sample) and cholesterol-d6 (cholest-5-en-3β-ol-D6; 1.455 μg/sample) were added as internal standards for quantification purposes. Hydrocarbons and sterols were separated via open column chromatography (SiO_2) using *n*-hexane and methylacetate:*n*-hexane (20:80 v/v), respectively. Sterols were silylated with 500 μl BSTFA (60 °C, 2 h) prior to analysis. Gas chromatography–mass spectrometry (GC–MS) compound analyses of both fractions were performed using an Agilent 6850 GC (30 m HP-5 ms column, 0.25 mm inner diameter, 0.25 μm film thickness) coupled to an Agilent 5975 C VL mass selective detector. The GC oven was heated from 60 °C to 150 °C at 15 °C min^{-1}, and then at 10 °C min^{-1} to 320 °C (held 15 min) for the analysis of hydrocarbons and at 3 °C min^{-1} to 320 °C (held 20 min) for sterols, respectively. Helium was used as carrier gas. Individual compound identification was based on comparisons of their retention times with that of reference compounds (applies to brassicasterol and *n*-alkanes) and on comparisons of their mass spectra with published data (Belt et al., 2007; Boon et al., 1979; Volkman, 1986). Biomarker concentrations were calculated on the basis of their individual GC–MS ion responses compared with those of respective internal standards. The quantification is based on the assumption that the ion yield is nearly identical for the analytes and the internal standards. All correlations of the monitoring ions for internal standards versus TIC (Total Ion Current) and versus concentration are highly satisfactory ($R^2 = 0.987–1$). IP_{25} was quantified using its molecular ion *m/z* 350 in relation to the abundant fragment ion *m/z* 266 of 7-hexylnonadecane and by means of an external calibration curve ($R^2 = 0.9989$). Brassicasterol (24-methylcholesta-5,22E-dien-3β-ol) and dinosterol (4α,23,24-trimethyl-5α-cholest-22E-en-3β-ol) were quantified as trimethylsilyl ethers

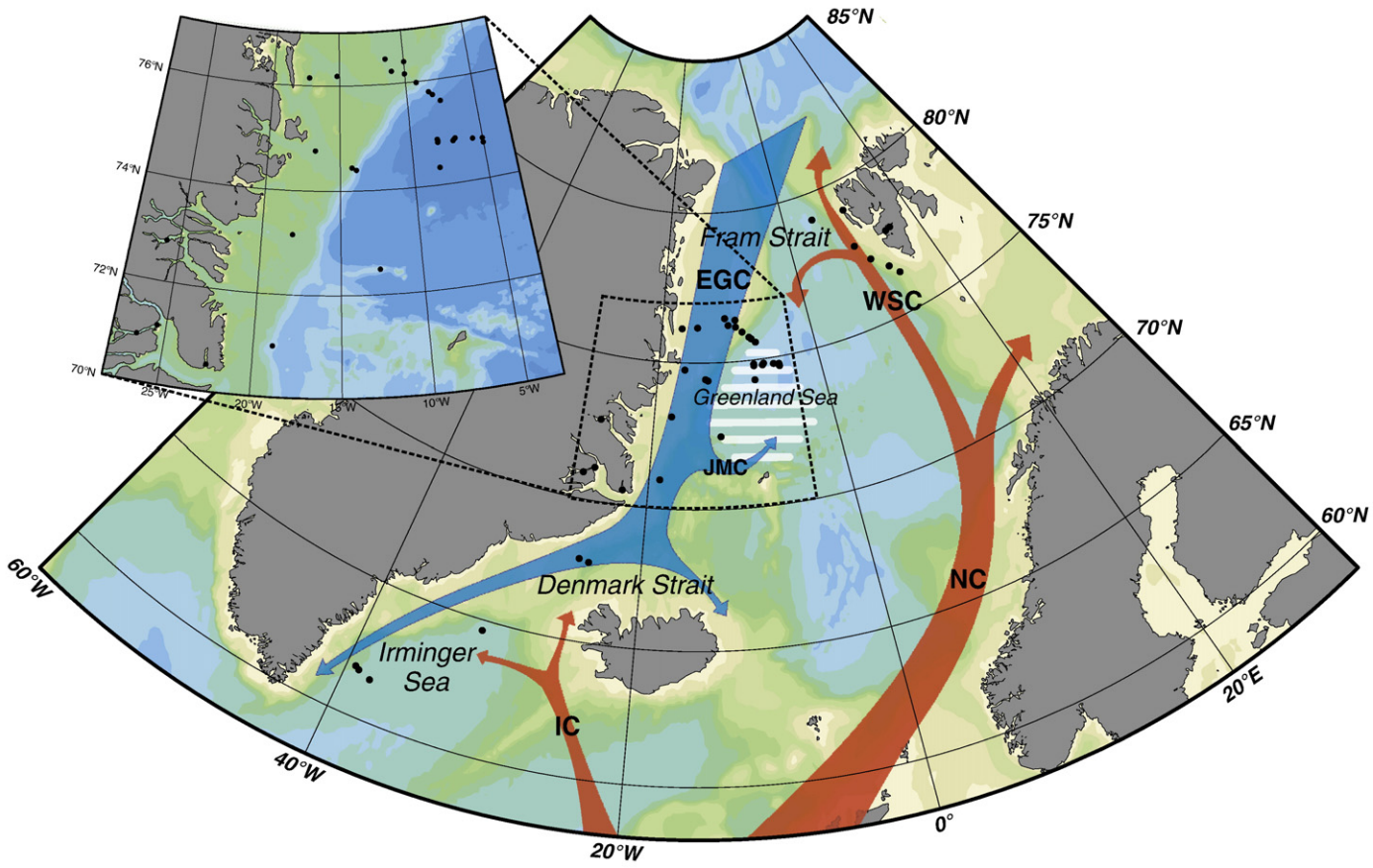

Fig. 1. Oceanographic setting in the study area (after Rudels et al., 2005) and locations of sampling sites (black dots). Red arrows refer to Atlantic Ocean derived warm surface waters: NC = Norwegian Current, WSC = West Spitsbergen Current, IC = Irminger Current. Blue arrows indicate Arctic Ocean derived cold surface waters: EGC = East Greenland Current, and JMC = Jan Mayen Current. White bars denote area of Odden ice tongue development.

using the molecular ions m/z 470 and m/z 500, respectively, and m/z 464 for cholesterol-d6. Fragment ion m/z 57 was used to quantify the short-chain n-alkanes (n-C_{15}, n-C_{17}, n-C_{19}) via squalane. Sterol concentrations and the calibration curve for quantifying IP_{25} have been verified by GC measurements. Finally, biomarker concentrations were corrected to the amount of extracted sediment.

With respect to individual sedimentary (facies) regimes within the study area, absolute biomarker concentrations have been normalised to total organic carbon contents (TOC; data from Birgel and Stein, 2004; Kierdorf, 2006) to compensate for different depositional and burial efficiencies. Sedimentation rates within fjords or at continental margins, for example, are two to three times higher than in the deep-sea (Dowdeswell and Cofaigh, 2002), which may cause a dilution of the biomarker content. Presenting biomarker concentrations per gramme sediment hence could result in an underestimation of the biomarker content of the respective sediments.

The pronounced concentration difference between phytoplankton markers and IP_{25} is likely attributable to the variety of source organisms that are known to synthesise short-chain n-alkanes, brassicasterol, and dinosterol (e.g. Blumer et al., 1971; Volkman et al., 1993, 1998). In contrast, IP_{25} seems to be exclusively produced by one distinct sea ice diatom species (Belt et al., 2007), which would explain for the comparatively low abundance of this trace compound.

3.2. Numerical model — experimental design

In order integrate sea ice within climate modelling, a dynamical downscaling from a coarse-resolution climate model (3.8°×3.8° horizontal resolution) to a high-resolved regional ocean–sea ice model (0.25° horizontal resolution) has been specifically designed for palaeo-modelling studies (see Supplementary Material S1 for detailed procedure). The coarse-resolution (T31L19) climate model simulations have been performed for present and Holocene conditions (Lorenz and Lohmann, 2004). The coarse-resolved SST and sea ice fields of Lorenz and Lohmann (2004) have been bilinearly interpolated to a finer resolved 1.1°×1.1° matrix and applied to a high-resolution version (T106L31) of the atmospheric circulation model ECHAM5 (Roeckner et al., 2006). Each high-resolution simulation covers 50 integration years, where the last 40 years are used as forcing for the regional North Atlantic/Arctic Ocean–Sea Ice Model (NAOSIM). NAOSIM has been developed to simulate present sea ice variability, circulation, and hydrography in the North Atlantic/Arctic realm (Gerdes et al., 2003; Karcher et al., 2003; Kauker et al., 2003). The model domain of NAOSIM encompasses the Arctic Ocean and adjacent North Atlantic seas (see Supplementary Fig. S2). Our employed model experiments have been carried out at a horizontal grid resolution of 0.25° and 30 vertical levels. Following Kauker et al. (2003), lateral ocean boundaries (volume flux, temperature, and salinity) have been set to present observations at 50°N in the North Atlantic and at 65°N in the Bering Strait. In order to get a realistic halocline in the Arctic Ocean, the ocean surface salinity is weakly restored (time-scale of 6 months) to the monthly sea surface salinity climatology (Steele et al., 2001). The modern and Mid Holocene NAOSIM runs are integrated over 100 model years, where the last 30 years are analysed in terms of sea ice coverage and thickness.

A detailed analysis of the Mid Holocene will be the subject of a forthcoming study.

Table 1
Station list and biomarker data. TOC data from Birgel and Stein (2004) and Kierdorf (2006). The P_BIP_{25} index for individual sampling sites has been calculated using a concentration balance factor (c).

Station Nr.	Latitude	Longitude	Water depth (m)	TOC (wt. %)	IP_{25} (μg/g OC)	Brassicasterol (μg/g OC)	Dinosterol (μg/g OC)	Σ n-C_{15}, n-C_{17}, n-C_{19} (μg/g OC)	P_BIP_{25} (c = 0.014)
PS57/127-1	79.0333	10.51	−307	1.87	0.76	234.22	47.15	55.41	0.19
PS57/130-1	77.7833	9.68	−388	0.86	0.85	108.52	25.57	153.67	0.36
PS57/131-2	77.1683	11.1	−320	0.83	0.59	129.33	26.25	167.31	0.25
PS57/136-2	77.81	15.8817	−589	1.68	0.28	93.35	8.09	221.20	0.18
PS57/137-2	77.77	15.065	−1442	2.11	0.41	100.42	14.15	127.56	0.23
PS57/138-1	76.6817	12.995	−1013	0.87	0.54	63.38	17.18	207.21	0.38
PS57/145-1	76.335	13.9283	−1502	1.19	0.17	85.54	16.93	115.79	0.13
PS57/166-2	79.13	4.893	−527	1.29	0.67	100.45	21.16	37.69	0.33
PS62/002-3	61.7947	−39.3738	−1928	0.2	0	201.45	30.77	13.58	0
PS62/003-3	61.701	−39.0676	−2192	0.23	0	686.33	73.10	17.10	0
PS62/004-2	61.5258	−38.1232	−2564	0.37	0	134.12	28.83	12.45	0
PS62/012-2	64.6243	−31.6933	−2431	0.23	0	111.09	19.14	18.04	0
PS62/015-4	67.9307	−25.4291	−1013	0.59	3.88	135.21	39.64	23.70	0.67
PS62/017-1	67.8508	−24.582	−1502	0.62	4.11	234.00	43.71	31.10	0.56
PS62/020-1	70.9989	−18.9151	−1374	0.64	2.59	116.60	22.06	40.63	0.62
PS62/022-3	72.4906	−12.6063	−527	0.71	1.65	152.59	27.60	44.23	0.44
PS62/026-3	74.332	−8.213	−3341	0.87	0.83	97.79	17.93	42.56	0.38
PS62/027-1	74.824	−7.008	−3510	0.77	0.82	93.70	16.91	31.38	0.39
PS62/028-1	74.849	−6.915	−3477	0.69	0.70	95.18	16.86	33.04	0.35
PS62/029-2	74.799	−7.084	−3471	0.64	0	70.93	15.86	24.08	0
PS62/038-1	74.767	−5.026	−3603	0.28	0	85.30	15.03	22.46	0
PS62/041-1	74.684	−5.012	−3602	0.67	0	101.85	17.70	29.05	0
PS62/044-1	74.7901	−5.6937	−3558	0.78	0.61	84.02	17.83	27.70	0.34
PS62/046-3	74.808	−8.152	−3395	0.75	0.87	101.84	23.49	43.73	0.38
PS62/048-1	74.841	−8.142	−3458	0.75	0.93	119.30	19.26	32.36	0.36
PS62/050-1	74.867	−8.154	−3383	0.7	0.97	95.52	21.12	28.87	0.42
PS64/487-1	76.149	−17.283	−234	0.53	6.40	72.86	24.86	9.78	0.86
PS64/488-1	76.1828	−15.181	−320	0.88	2.43	35.44	12.10	16.76	0.83
PS64/489-1	76.2356	−11.0017	−315	0.44	2.77	77.81	16.23	16.92	0.72
PS64/490-1	76.397	−9.9913	−264	0.27	3.47	86.95	28.52	28.03	0.74
PS64/504-1	75.7209	−8.0882	−2324	0.39	1.23	63.49	18.41	32.62	0.58
PS64/508-1	75.9817	−9.1974	−1087	0.4	1.48	30.33	10.20	26.97	0.78
PS64/511-1	76.1658	−10.0127	−288	0.44	1.96	67.15	17.37	13.51	0.68
PS64/516-1	76.4749	−11.4143	−314	0.62	1.38	54.61	14.27	8.37	0.65
PS64/528-1	75.5895	−7.5765	−3187	0.58	0.66	33.73	9.10	17.14	0.59
PS64/531-1	75.7817	−8.3472	−2023	0.54	1.29	55.93	18.96	41.91	0.62
PS64/573-1	74.765	−16.7318	−388	1.02	2.72	59.81	19.88	21.44	0.77
PS64/582-1	74.4423	−14.1948	−589	0.44	2.28	65.28	19.93	26.01	0.72
PS64/583-2	74.3977	−13.8936	−1442	0.51	1.47	48.59	13.65	42.03	0.69
PS2630-7	73.16	−18.0683	−287	0.32	4.89	127.24	32.81	26.88	0.74
PS2642-2	72.79	−25.8217	−759	0.1	8.47	217.63	51.80	16.49	0.74
PS2648-3	70.525	−22.51	−109	0.69	3.77	202.29	31.80	83.65	0.57
PS2651-3	71.15	−25.5417	−773	0.14	2.60	251.33	63.88	18.73	0.43
PS2654-6	70.9217	−26.5833	−942	0.13	3.51	234.65	66.11	14.22	0.52

4. Results and discussion

4.1. Biomarker data: autochthonous versus allochthonous signal

With reference to the particular ice drift and dynamic current system in the study area, input of allochthonous matter and lateral advection of organic material demand consideration as they potentially affect the accumulation and composition of the biomarker assemblages investigated herein. For example, the allochthonous input of lithogenic and organic particles entrained in sea ice, which may originate from the shallow shelves of the Laptev Sea (Eicken et al., 1997; Nürnberg et al., 1994; for a recent review see Stein, 2008), probably impacts on the biomarker content of sediments from the East Greenland shelf. In terms of absolute IP_{25} concentrations, we thus suggest that a blend of in-situ produced and allochthonous IP_{25} should be considered. Nonetheless, the occurrence of IP_{25} in these sediments strongly indicates the former presence (and melt) of (drift) sea ice. As we notice that no correlation exists between phytoplankton biomarker and sea ice concentrations (see Supplementary Fig. S3), we assume that the allochthonous input of brassicasterol, dinosterol, and short-chain *n*-alkanes via sea ice seem to be of less importance in the study area.

Sedimentary biomarker contents also depend on the fate of the sea surface derived organic material (1) on its way towards and (2) at the sea floor as, for instance, lateral advection by subsurface currents, biodegradation or the physical/chemical alteration of organic matter may imprint on the preservation of biomarker lipids (see Zonneveld et al., 2010 and references therein). However, given that we do not observe a distinct correlation between the water depth at the individual sampling sites and their biomarker contents (see Supplementary Fig. S4) and that the distribution of IP_{25} and the phytoplankton markers display the modern sea surface conditions reasonably well (see Section 4.2), we suggest that the organic matter is effectively transported through the water column. The (concurrent) release of fine-grained lithogenic material during the ice melt in the study area supports the formation of organic-mineral aggregates (and zooplankton faecal pellets; Bauerfeind et al., 2005), which notably accelerates the downward transport of organic matter towards the seafloor. This provides for a rapid sedimentation of the biomarker lipids and reduces their residence time at the sediment-water interface, where degradation takes place (Bauerfeind et al., 2005; Knies, 2005; Stein, 1990). Finally, besides indicating a lack of sea ice coverage, the absence of IP_{25} in surface sediments from the Irminger Sea – the major discharge area for Denmark Strait Overflow Water (Rudels et al.,

2005) – substantiates that relocation of biomarker signals by (sub) surface currents seems to be negligible – at least in this part of the study area. Thus, we interpret our biomarker data as direct proxies for sea ice cover and surface water productivity.

4.2. Biomarker distribution: sea ice conditions and sea surface primary productivity

Concentrations of IP_{25} and phytoplankton specific biomarker lipids (short-chain *n*-alkanes, brassicasterol and dinosterol; for review see Volkman (2006)) determined on surface sediments from the continental margins of East Greenland and West Spitsbergen are visualised by means of the Ocean Data View Software 4.2.1 (Fig. 2a–d; Schlitzer, 2009; for biomarker concentrations see also Table 1).

Highest IP_{25} concentrations are found in sediments from the East Greenland fjords (3.5–8.5 μg/g OC), along the proximal shelf of northeast Greenland (2.3–6.4 μg/g OC) and in the two samples from Denmark Strait (ca. 4 μg/g OC; Fig. 2a) and likely refer to an extended (lasting throughout spring and early summer) sea ice cover at these sites. Furthermore, these elevated IP_{25} concentrations align well with microfossil data from Matthiessen et al. (2001) and Andersen et al. (2004), who report on the dominance of polar dinoflagellate cysts and sea ice diatom assemblages in sediments underlying the ice-covered polar water masses along the East Greenland shelf. North of 75°N this sea ice lasts until summer (Gloersen et al., 1992) and hence hampers phytoplankton productivity, which explains for the minimum concentrations of short-chain *n*-alkanes (<30 μg/g OC), brassicasterol (<60 μg/g OC), and dinosterol (<20 μg/g OC) in these sediments (Fig. 2b–d).

Gradually reduced IP_{25} contents in samples from the distal East Greenland shelf (2–3.5 μg/g OC) and the continental slope (1.2–2.6 μg/g OC) suggest less intense or variable ice conditions towards the east. This is consistent with findings of Koç Karpuz and Schrader (1990) who observed an eastward shift in the geographic distribution of a sea ice diatom assemblage (dominant at the shelf) towards an Arctic water diatom assemblage (dominant along the continental margin). Similarly, Pflaumann et al. (1996) found an eastward decrease in the abundance of the polar planktic foraminifer *Neogloboquadrina pachyderma* (sin.).

A north–south gradient of generally low IP_{25} concentrations in sediments from eastern Fram Strait (0.2–0.8 μg/g OC; Fig. 2a) likely reflects the influence of warm Atlantic water carried by the WSC along the West Spitsbergen shelf towards the north. Minimum IP_{25} concentrations at the southern part of the West Spitsbergen shelf thus point to minor sea ice occurrences. At these sites, the still remarkable heat content of the Atlantic water reduces the formation of sea ice during autumn and accelerates its melt during spring/summer. The growth of phytoplankton consequently benefits from these mainly ice-free conditions and is reflected in significantly elevated contents of short-chain *n*-alkanes (40–220 μg/g OC), dinosterol (20–50 μg/g OC), and – to a lower extent – brassicasterol (90–230 μg/g OC; Fig. 2b–d). Likewise, elevated TOC values determined on surface sediments from eastern Fram Strait are related to a higher surface water productivity caused by warm WSC waters (Birgel et al., 2004; Hebbeln and Berner, 1993).

Diminished concentrations of both IP_{25} (<1 μg/g OC) and phytoplankton biomarkers in sediments from the northern Greenland Sea (off the East Greenland continental margin; ca. 75°N), however, are

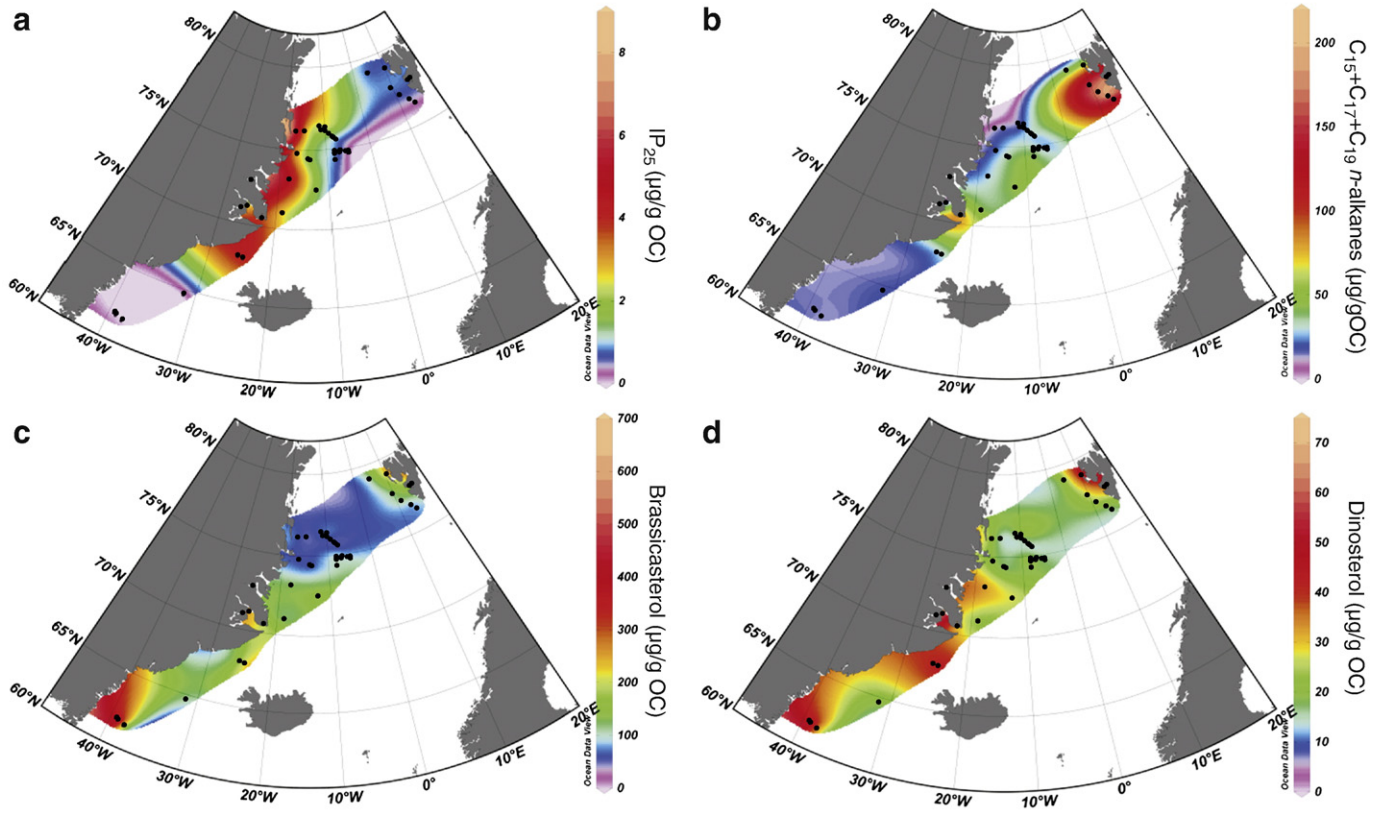

Fig. 2. Concentrations of the sea ice proxy IP_{25} (a) and phytoplankton-derived biomarkers (short-chain *n*-alkanes (b), brassicasterol (c), and dinosterol (d)) in surface sediments from the continental margins of East Greenland and West Spitsbergen. Maps are generated with the Diva Gridding Algorithm supplied by the Ocean Data View software package (Schlitzer, 2009). Note that on concentration scales absolute values are given equidistantly whilst colours are automatically adjusted to accentuate concentration gradients.

possibly attributable to unsuitable environmental conditions. The (spring) sea ice cover in the Odden ice tongue area mainly consists of newly formed frazil and pancake ice (Comiso et al., 2001), which, in comparison to multiyear sea ice, presumably does not accommodate high amounts of sea ice diatoms (synthesising IP_{25}). Furthermore, the highly variable ice conditions with a rapidly (within days) oscillating ice-edge position and high salinity fluxes that result from brine expulsion (Comiso et al., 2001; Gloersen et al., 1992) may negatively impact on the spring primary productivity. Limited nutrient availability due to the gyre-like surface circulation within the Greenland Sea and thus isolation from external supply of nutrients as suggested by Rey et al. (2000), may also account for reduced phytoplankton biomarker abundances.

In contrast, the co-occurrence of increased IP_{25} and phytoplankton biomarker contents along the distal shelf of East Greenland (<74°N) and at Denmark Strait indicates favourable living conditions for both ice algae and open-water phytoplankton. We thus conclude that these areas confine a more or less stable (i.e. lasting from spring to summer) ice-margin regime as an advantageous living habitat for both algal species. This is consistent with the findings of Smith et al. (1987) and Sakshaug (2004) who demonstrated previously that marine primary productivity is enhanced at the ice-edge due to a stabilisation of the water column and increased nutrient release from melting sea ice (for "marginal ice zone" carbon fluxes see also Wassmann et al., 2004). Further studies in the Greenland Sea highlighted maximum phytoplankton biomass and chlorophyll-*a* concentrations in the vicinity of the ice edge (Richardson et al., 2005; Smith et al., 1985). Higher sedimentary TOC values and elevated fluxes of particulate organic carbon and biogenic silica are also described by Kierdorf (2006), Ramseier et al. (1999) and Peinert et al. (2001) from the marginal ice zone along the continental margin of East Greenland, which supports our assumption of a "high productive" ice-edge corridor along the outer shelf.

No IP_{25} could be detected in the sediments from the Irminger Sea (<65°N; Fig. 2a). Since brassicasterol and dinosterol are enriched in these samples (130–680 μg/g OC and 30–73 μg/g OC, respectively), thus suggesting a satisfactory environmental setting for open-water phytoplankton (i.e. diatoms, coccoliths, and dinoflagellates as main source organisms of brassicasterol and dinosterol; Volkman, 1986 and references therein; Volkman et al., 1993), we conclude that the absence of IP_{25} results from a considerably reduced formation and/or advection of sea ice at these sites (Lisitzin, 2002; Ramseier et al., 2001). The generally low concentrations of short-chain *n*-alkanes in these surface sediments, however, may refer to less favourable ecological conditions (nutrient depletion, grazing pressure) for the respective short-chain *n*-alkane synthesising algae (mainly brown-, red-, green-algae; Blumer et al., 1971; Gelpi et al., 1970).

4.3. Phytoplankton-IP_{25} index

Including a phytoplankton component to assess sea ice conditions occurs reasonable since sea ice evidently acts not only as a limiting factor for phytoplankton growth (as demonstrated for the marginal ice zone along the continental margin of East Greenland). The risk to overestimate sea ice coverage purely on the base of high IP_{25} concentrations thus can be reduced. Similarly, an underestimate of sea ice coverage deduced from the absence of IP_{25}, which in fact may also result from a permanent ice cover (Belt et al., 2007; Müller et al., 2009), can be circumvented, when the content of phytoplankton markers is known (for a first application of this combinatory approach within a palaeo sea ice study see Müller et al., 2009). Fig. 3 provides a generalised overview about sea ice conditions and the corresponding productivity of sea ice algae and phytoplankton at the sea surface; respective biomarker fluxes towards the sea floor are indicated too. We propose that by means of the sedimentary biomarker contents a phytoplankton-IP_{25} index (PIP_{25}) can be calculated, which gives the fraction of IP_{25} to the combined IP_{25} and phytoplankton marker content. Since we herein observed a significant concentration difference between IP_{25} and phytoplankton derived biomarkers, and we assume that this may also account for other marine environments

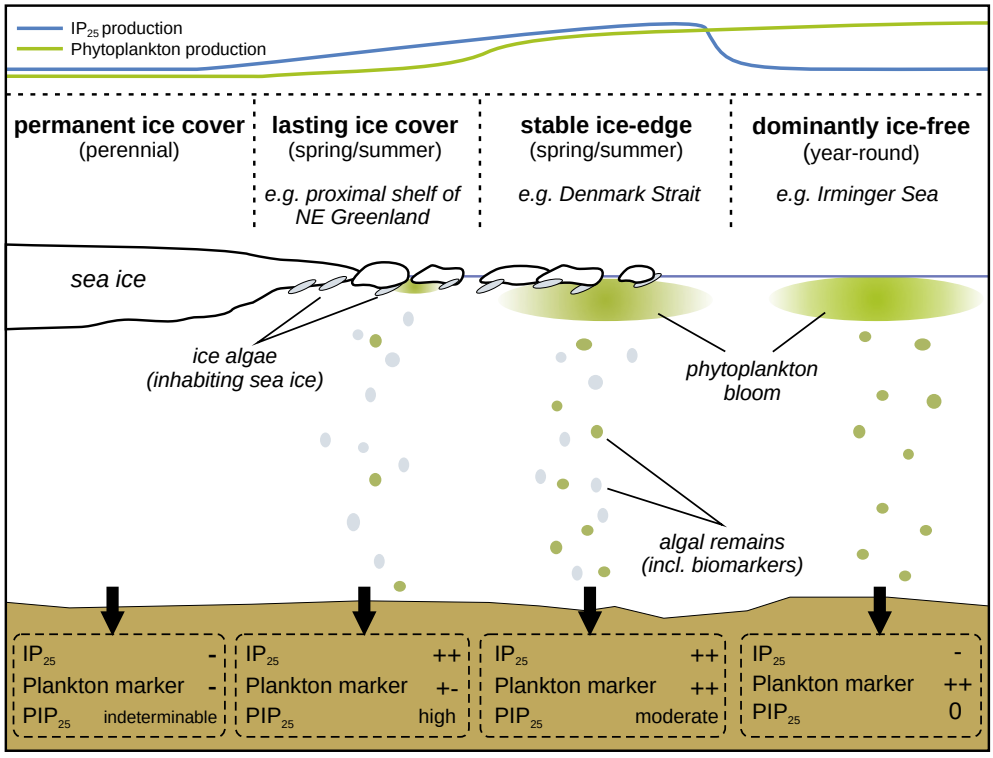

Fig. 3. Generalised scheme illustrating distinct sea surface conditions and respective (spring/summer) productivities of ice algae and phytoplankton. Overview sedimentary contents of IP_{25} and the phytoplankton-derived biomarkers and resulting PIP_{25} indices are indicated for each setting.

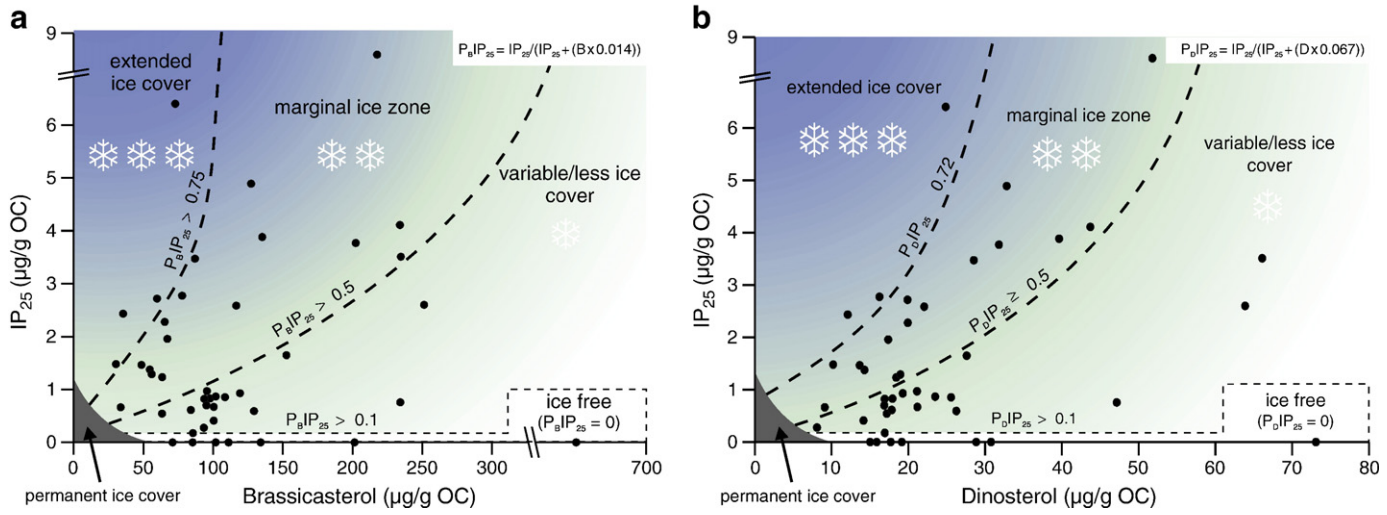

Fig. 4. Correlation of IP_{25} versus brassicasterol (a) and dinosterol concentrations (b) and corresponding P_BIP_{25} and P_DIP_{25} indices calculated for sediments from the study area by means of respective equations (upper right corner within each panel). The light-green to blue shaded background fields and snow symbols indicate the transition from minimum to maximum sea ice coverage. Note that permanent ice cover (dark grey field) is not observed herein.

in the Arctic, we recommend that a concentration balance factor (c) needs to be considered for the calculation of this PIP_{25} index:

(1) $PIP_{25} = IP_{25}/(IP_{25} + (\text{phytoplankton marker} \times c))$ with
(2) c = mean IP_{25} concentration / mean phytoplankton biomarker concentration.

The PIP_{25} index accounts for the (spring/summer) algal activity beneath the sea ice (mainly ice algae), at the ice-edge (ice and phytoplankton algae), and in ice-free areas (phytoplankton) and thus allows a rough estimate of the spatial and temporal extent of the sea ice cover (Fig. 3). High PIP_{25} values accordingly refer to high sea ice cover, whilst low values point to a reduced sea ice cover. With respect

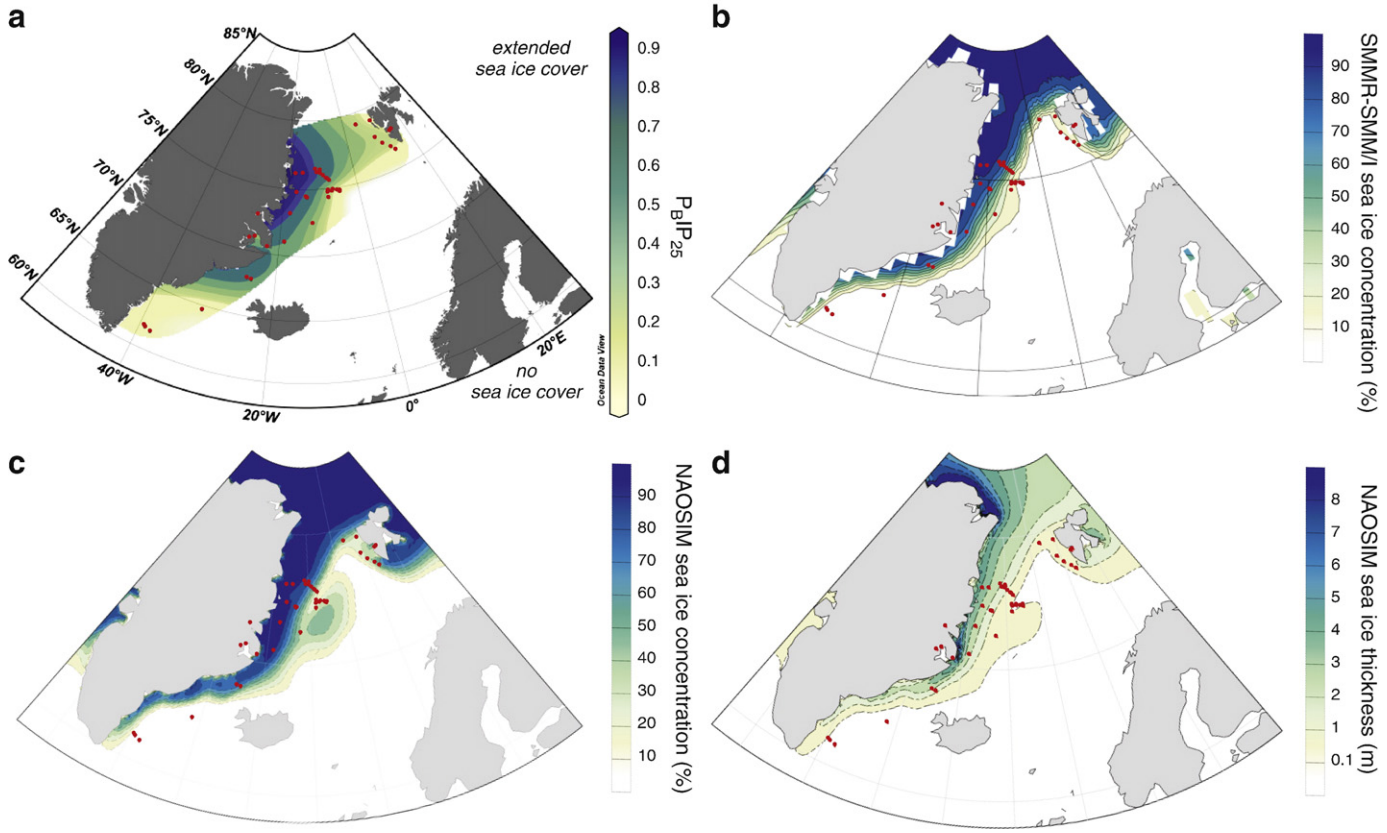

Fig. 5. Comparison of the (a) biomarker-based estimate of sea ice coverage using the P_BIP_{25} index with (b) SMMR-SSM/I satellite derived mean spring sea ice concentrations, (c) NAOSIM modelled spring sea ice concentrations, and (d) sea ice thicknesses. Both satellite and NAOSIM-based sea ice data are averaged over the period from 1979 to 2003. Red dots denote sites of sediment samples.

to the variety of phytoplankton biomarkers we propose that this PIP_{25} index should be appropriately specified through indices, for example as P_BIP_{25} or P_DIP_{25} when using brassicasterol or dinosterol. The use of such an index to distinguish between different sea ice conditions, however, requires essential awareness of the individual biomarker concentrations to avoid misleading interpretations. For instance, coevally high amounts of both biomarkers (suggesting ice-edge conditions) as well as coevally low contents (suggesting permanent-like ice conditions) would give the same PIP_{25} value.

A correlation of IP_{25} versus brassicasterol and dinosterol concentrations in sediments from the study area is given in Fig. 4, where we also denote different zones of sea ice conditions with corresponding P_BIP_{25} and P_DIP_{25} values calculated for the surface samples. Conveniently, such an index also facilitates the graphic representation of the environmental information carried by the ice proxy and the phytoplankton marker as shown for the P_BIP_{25} values (Fig. 5a). Maximum P_BIP_{25} values (dark blue contour lines in Fig. 5a; $P_BIP_{25} \pm 0.85$) indicate pronounced ice coverage throughout the spring and summer season as found along the proximal shelf of NE Greenland, whereas an index of 0 (no IP_{25}; pale yellow contours in Fig. 5a) suggests pre-dominantly ice-free conditions as, for example, at the sampling sites in the Irminger Sea. Accommodating living conditions for ice algae and open-water phytoplankton characterise the marginal ice zone (with a relatively stable ice edge lasting from spring to summer) along the distal shelf of East Greenland towards Denmark Strait (dark-green contours; $P_BIP_{25} \pm 0.65$). Light-green contours ($P_BIP_{25} \pm 0.25$) finally denote a short-lasting maximum sea ice extent with notably lowered ice concentrations in the north-eastern Greenland Sea (at ca. 75°N) and along the West Spitsbergen margin (Fig. 5a).

We point out that using dinosterol or short-chain *n*-alkane contents (instead of brassicasterol) for the calculation of respective P_DIP_{25} and $P_{Alk}IP_{25}$ indices yields basically similar results (see Supplementary Fig. S5). That means that these biomarker ratios could be used to qualitatively estimate sea ice coverage as well, though we note that the $P_{Alk}IP_{25}$ index seems to somewhat overestimate the sea ice coverage, for example, in the Denmark Strait. Since the P_BIP_{25} values show a slightly higher correlation with sea ice concentrations determined by satellite imagery than the P_DIP_{25} index we herein used the P_BIP_{25} index for reconstructions of sea ice conditions in the study area.

4.4. Comparison of biomarker and satellite sea ice data

The SMMR (NIMBUS-7 satellite) and SSM/I (DMSP satellites) based sea ice map (Fig. 5b) shows mean (spring) sea ice concentrations derived from the AMSR-E Bootstrap Algorithm (Cavalieri et al., 1996 (updated 2008)). Monthly (March–April–May) mean sea ice concentrations have been averaged for the period from 1979 to 2003. Certainly, a one-to-one comparison of sea ice conditions obtained from satellite observations (displaying a 25 years mean) with estimates based on sediment data is flawed by the different time frames that are captured by both methods. Depending on sedimentation rates, surface sediments from the study area may easily represent a much longer time interval (decades to centuries) — this needs to be kept in mind. The problematic age control is also common to other "modern analogue" geochemical or microfossil studies (de Vernal et al., 2001; Müller et al., 1998) and can partly be solved by ^{14}C age determinations of the respective sediments only (Pflaumann et al., 2003).

Remote sensing imagery indicates highest sea ice concentrations (about 100%) at the northernmost and western part of Fram Strait along the EGC affected continental margin of Greenland (Fig. 5b). This aligns with maximum IP_{25} concentrations in the respective sediments. A gradual eastward decline in sea ice concentrations (from highest to lowest values) is observed along the polar front paralleling the continental slope of East Greenland, which is also reflected in the biomarker data. Minimum to zero ice concentrations within the Greenland Sea could explain for the general low contents of IP_{25} and also its absence in some of these surface sediments (Fig. 2a). Similarly, sampling sites south of Denmark Strait (in the Irminger Sea) are located in virtually ice-free waters (Fig. 5b), which is also reflected in the absence of IP_{25}.

For a more quantitative comparison of the biomarker and satellite data we used the sea ice concentrations as they are displayed for the individual sediment sampling sites (Fig. 5b; Table 2). As expected, IP_{25} concentrations correlate positively with ice coverage (Fig. 6a; $R^2 = 0.67$). This correlation, however, may importantly highlight the fundamental ambiguity of the sea ice proxy, as, for example, relatively low IP_{25} contents are observed not only for minimum but also maximum ice coverage (Fig. 6a). Sedimentary IP_{25} contents hence should not be used as a direct measure for sea ice concentrations. This and also the higher correlation of P_BIP_{25} values with sea ice concentrations (Fig. 6b; $R^2 = 0.74$) strengthens that the coupling of IP_{25} with a plankton marker (e.g. brassicasterol) proves to be a valuable and more reliable approach for realistic sea ice reconstructions.

Table 2
Station list with satellite (SMMR-SSM/I) derived (spring) sea ice concentrations (±5%) and NAOSIM modelled (spring) sea ice concentrations (±5%) and ice thicknesses (±0.5 m). Data are averaged over the period from 1979 to 2003. n.d.: no data.

Station Nr.	Latitude	Longitude	Satellite sea ice concentration (%)	NAOSIM sea ice concentration (%)	NAOSIM sea ice thickness (m)
PS57/127-1	79.0333	10.51	15	25	0.5
PS57/130-1	77.7833	9.68	5	25	0.5
PS57/131-2	77.1683	11.1	5	25	0.5
PS57/136-2	77.81	15.8817	n.d.	n.d.	n.d.
PS57/137-2	77.77	15.065	n.d.	n.d.	n.d.
PS57/138-1	76.6817	12.995	15	35	0.5
PS57/145-1	76.335	13.9283	15	45	0.5
PS57/166-2	79.13	4.893	15	35	0.5
PS62/002-3	61.7947	−39.3738	5	5	0
PS62/003-3	61.701	−39.0676	5	5	0
PS62/004-2	61.5258	−38.1232	5	5	0
PS62/012-2	64.6243	−31.6933	5	5	0
PS62/015-4	67.9307	−25.4291	65	75	1.5
PS62/017-1	67.8508	−24.582	45	65	0.5
PS62/020-1	70.9989	−18.9151	65	95	2.5
PS62/022-3	72.4906	−12.6063	25	35	0.5
PS62/026-3	74.332	−8.213	15	35	0.5
PS62/027-1	74.824	−7.008	15	25	0
PS62/028-1	74.849	−6.915	15	25	0
PS62/029-2	74.799	−7.084	15	25	0
PS62/038-1	74.767	−5.026	5	35	0.5
PS62/041-1	74.684	−5.012	5	35	0.5
PS62/044-1	74.7901	−5.6937	5	35	0.5
PS62/046-3	74.808	−8.152	15	25	0
PS62/048-1	74.841	−8.142	15	25	0
PS62/050-1	74.867	−8.154	15	25	0
PS64/487-1	76.149	−17.283	95	95	3.5
PS64/488-1	76.1828	−15.181	95	95	2.5
PS64/489-1	76.2356	−11.0017	85	85	1.5
PS64/490-1	76.397	−9.9913	75	75	1.5
PS64/504-1	75.7209	−8.0882	25	35	0.5
PS64/508-1	75.9817	−9.1974	55	45	0.5
PS64/511-1	76.1658	−10.0127	65	75	1.5
PS64/516-1	76.4749	−11.4143	85	85	1.5
PS64/528-1	75.5895	−7.5765	25	25	0.5
PS64/531-1	75.7817	−8.3472	35	45	0.5
PS64/573-1	74.765	−16.7318	85	95	2.5
PS64/582-1	74.4423	−14.1948	65	75	1.5
PS64/583-2	74.3977	−13.8936	65	75	1.5
PS2630-7	73.16	−18.0683	85	95	2.5
PS2642-2	72.79	−25.8217	n.d.	n.d.	n.d.
PS2648-3	70.525	−22.51	n.d.	75	5.5
PS2651-3	71.15	−25.5417	n.d.	n.d.	n.d.
PS2654-6	70.9217	−26.5833	n.d.	n.d.	n.d.

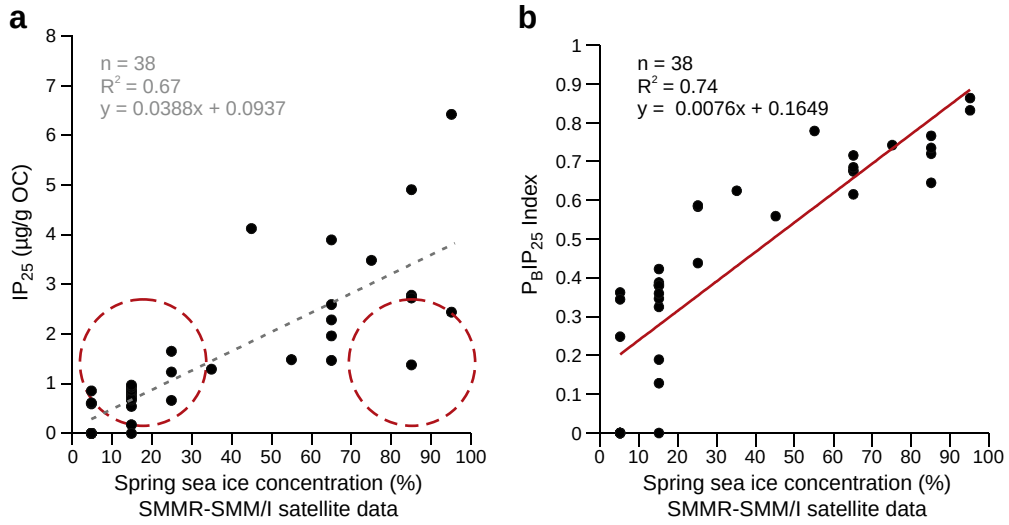

Fig. 6. Correlation of spring sea ice concentrations (±5%) derived from satellite data (SMMR-SSM/I; 1979–2003) with (a) IP_{25} concentrations and (b) P_BIP_{25} values. Coefficients of determination (R^2) are given for the respective regression lines. Red dashed circles highlight low IP_{25} concentrations, which misleadingly may be interpreted as indicative of low sea ice concentrations though they result from severe sea ice coverage limiting ice algae growth at the bottom of the ice.

4.5. Modelled sea ice distribution

The NAOSIM (spring) sea ice concentrations and thicknesses in the study area have been simulated for modern (1979–2003; Fig. 5c and d) and Mid Holocene conditions (see Supplementary Fig. S6).

Modelled sea ice cover and satellite-derived data yield largely consistent regional patterns. North of Fram Strait, Greenland, and Spitsbergen, the ice cover occurs to be almost 100% everywhere. Within the Fram Strait area, NAOSIM sea ice concentrations reveal a positive westward gradient with maximum concentrations of up to 100% at the East Greenland coast (Fig. 5c). These maximum sea ice concentrations are in good agreement with the development of extensive landfast ice over the shelf of NE Greenland (Hughes et al., 2011). As also observed via satellite, ice concentrations are reduced to 10% at the lowest at the western coastline of Spitsbergen. Along the proximal shelf of East Greenland, the model reproduces a band of high sea ice concentrations (approximately 90% to 100%) extending far to the south (70°N), thus mirroring the path of the EGC. South of 70°N, ice concentrations near the Greenland shoreline are still in the range of 60% to 80%, however, with a steeper decreasing gradient towards the south. The model depicts a gradual eastward decrease in sea ice concentrations (from 100% to 10%) to parallel the continental shelf break of East Greenland, as is also observed via satellite (Fig. 5b). To the east of the EGC affected shelf, between 70° and 76°N, an exposed patch of sea ice coverage (10% to 40% ice concentration) successfully represents the Odden ice tongue that results from the anticlockwise ocean gyre circulation of the Jan Mayen Current within the Greenland Sea (Wadhams et al., 1996). In the satellite image (Fig. 5b) this tongue-shaped protrusion of Odden ice, however, appears less pronounced with regard to its extent and also concentration-wise (0%–20%) than calculated by the model. The NAOSIM also tends to slightly overestimate the sea ice concentration north of Iceland and along the continental margin of West Spitsbergen by ca. 10%. Correlation analysis of satellite-based and modelled sea ice concentrations as they prevail at 38 of the 44 sediment-sampling sites (both satellite and model do not resolve conditions within fjords), however, reveals that the two data sets are in good agreement ($R^2 = 0.89$; Fig. 7).

Modelled ice thicknesses (Fig. 5d) pinpoint highest values of 7 to 9 m at the northern coast of Greenland (>80°N), consistent with the local accumulation of very thick multiyear sea ice and the formation of pressure ridges enforced by the wind-driven surface circulation in this area (Haas et al., 2006; Wadhams, 1990). In contrast, significantly lowered ice thicknesses in the eastern Fram Strait (0.5–1 m) likely reflect the impact of warm Atlantic water carried northwards by the WSC. Moderate ice thicknesses of about 3 to 4 m parallel the coast and proximal shelf of East Greenland (between 80° and 70°N) and are gradually reduced in a south-eastward direction (Fig. 5d). This general reduction in ice thicknesses is in good agreement with the findings of Wadhams (1992, 1997), who reported a continuous decline in the mean ice thicknesses with decreasing latitude from the northern Fram Strait (up to 4 m ice draft) towards the Greenland Sea (less than 1 m ice draft). Modelled ice thicknesses also align with observations from upward looking sonars located at 79°N, 5°W in the Fram Strait, which document mean spring sea ice thicknesses of 2.8 to 3.2 m for the period 1990–1994 (Vinje et al., 1998). Across the Greenland Sea, a patch of sea ice thickness of around 0.1 to 1 m is detached from the nearshore sea ice field. This pattern is consistent with the recognised field of sea ice concentrations in Fig. 5c.

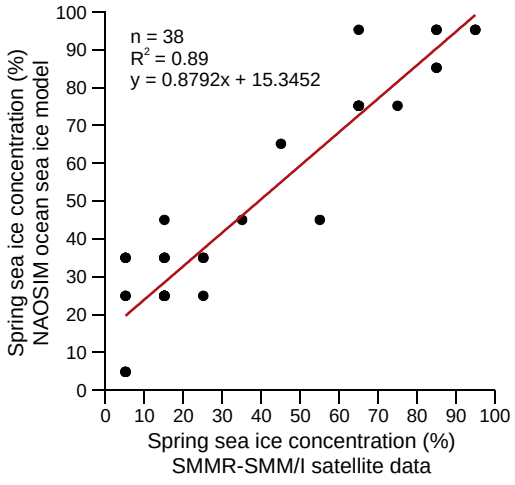

Fig. 7. Correlation of spring sea ice concentrations derived from satellite (SMMR-SSM/I) data and NAOSIM. Data points reflect sea ice concentrations (±5%) as determined at sediment sampling sites.

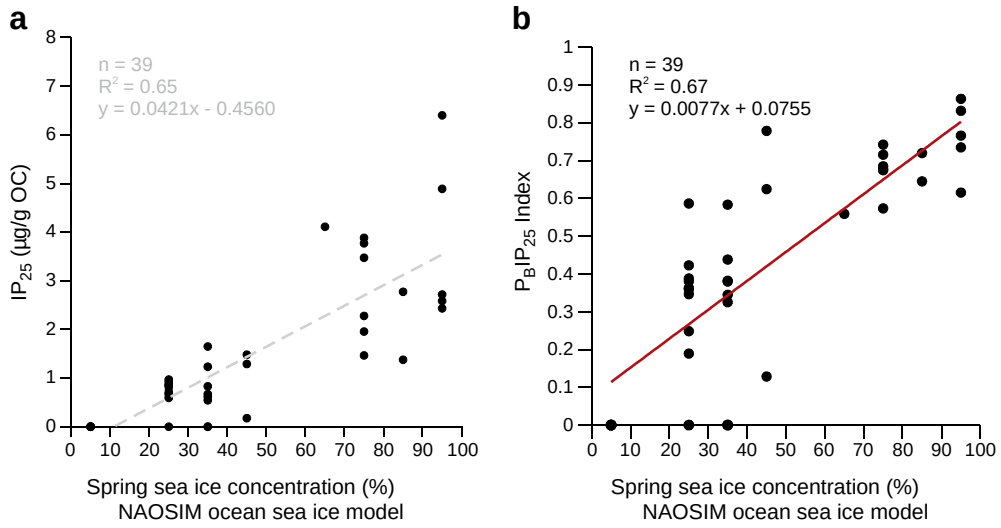

Fig. 8. Correlation of NAOSIM modelled spring sea ice concentrations (±5%) with IP_{25} contents (a) and P_BIP_{25} values (b). Coefficients of determination (R^2) are given for the respective regression lines.

Simulations of the palaeo modelling experiment suggest that (spring) sea ice concentrations and thicknesses in the study area were basically lower during the Mid Holocene than during modern times (Fig. S6). Particularly in eastern Fram Strait, sea ice concentrations were significantly reduced, which may point to an intensified Atlantic water inflow at this time. A detailed analysis of the Mid Holocene, however, is beyond the scope of this study, though a comparison of modelled and reconstructed sea ice parameters for past climates like the Mid Holocene would be a logical next step.

4.6. Proxy and model data: qualitative and quantitative comparisons

A rough qualitative comparison of the biomarker-based estimate of sea ice coverage (Fig. 5a) with model results exhibits a comparable pattern of the sea ice distribution in the study area with maximum sea ice cover along the proximal shelf of East Greenland, reduced sea ice cover along the West Spitsbergen continental slope and ice free conditions in the Irminger Sea. However, we also identify some inconsistencies between the modelled and proxy-based sea ice reconstruction. Unlike the model, which reproduces low to medium sea ice concentrations in the Odden ice tongue area, the P_BIP_{25} index seems to be less suitable to reflect the distribution of newly formed sea ice. Furthermore, maximum ice thicknesses at the outlet of the Scoresby Sund fjord system (East Greenland) are not supported by the biomarker data. According to the model, this sampling site experienced severe ice cover with more than 5 m ice thickness. But, instead of a hampered primary productivity (due to the limited light availability below the thick ice cover), we find enhanced contents of phytoplankton markers and IP_{25} in the respective sediment sample, indicating stable ice-edge conditions. Apparently, the ice cover was not completely closed at the fjord's mouth.

With regard to the general need of linking proxy and model approaches for palaeo reconstructions we herein provide a quantitative cross-evaluation of our biomarker and model results. Modelled sea ice concentrations correspond moderately with IP_{25} contents (Fig. 8a; $R^2 = 0.65$) and slightly stronger with P_BIP_{25} values (Fig. 8b; $R^2 = 0.67$), which again supports the assumption that this ratio reflects sea ice coverage more properly than the IP_{25} signal alone. In contrast, IP_{25} concentrations correlate more clearly with modelled ice thicknesses than the P_BIP_{25} values (Fig. 9). We assume that this

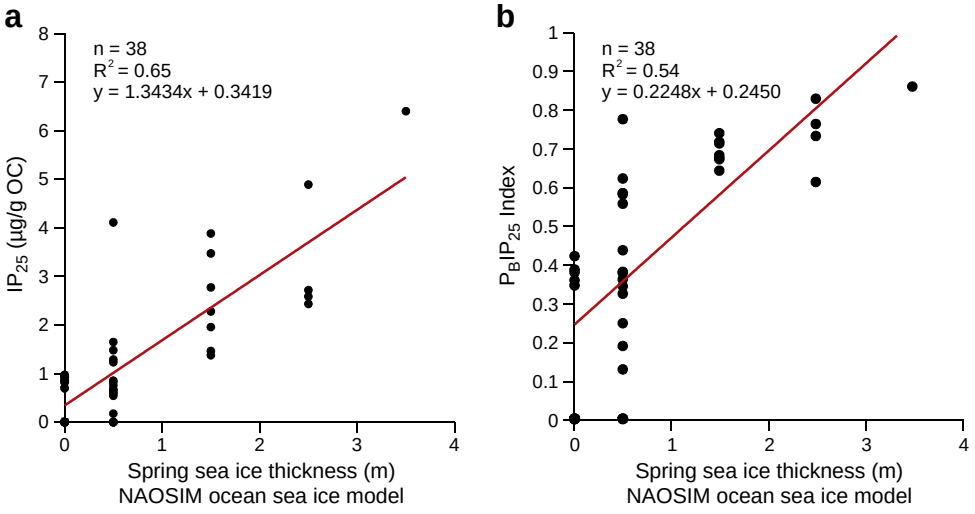

Fig. 9. Correlation of NAOSIM modelled spring sea ice thicknesses (±0.5 m) with (a) IP_{25} concentrations and (b) P_BIP_{25} values. Coefficients of determination (R^2) are given for the respective regression lines. From this correlation we excluded one outlying data point, which derives from the sediment sample located at the outlet of the Scoresby Sund fjord system.

indicates a non-linear response of (lower) phytoplankton activity to increasing ice thickness. The higher correlation between IP_{25} contents and ice thickness is probably due to the allochthonous transport of IP_{25} within thicker multi-year sea ice.

The largely good correlations of NAOSIM modelled sea ice concentrations with P_BIP_{25} values, however, occur rather enticing with regard to a quantitative proxy-model calibration. And though we surely acknowledge the utility of such a "sea-ice formula", i.e. the possibility to calculate absolute sea ice concentrations or thicknesses on base of biomarker data, we herein recognise few points that (hitherto) give concern about the applicability of this calibration. These are (1) the highly dynamic drift-ice component and hence the hardly assessable allochthonous input of organic matter (a transfer function based on the herein observed biomarker distribution, presumably would not be applicable to other Arctic sea ice environments); (2) the unknown age of the herein analysed sediments (do they reflect sea ice conditions of the past decades or centuries?); and (3) the relatively poor data base ($n=39$) and the scatter of data points within correlation charts, which entails a notable degree of uncertainty. We thus suggest that such a proxy-model calibration requires a larger biomarker dataset with a higher spatial distribution of sediment samples (ideally covering the whole Arctic Ocean). More IP_{25} studies on marine surface (and down-core) sediments from the Arctic realm will firstly provide for a validation of the P_BIP_{25} index and secondly provide for a valuable database to support (palaeo) model experiments. This would finally allow for a comparison of the herein included Mid Holocene sea ice model results (Fig. S6) with the respective Holocene sediment data. Once the reliability of this biomarker approach has been verified through further investigations it may enable for a quantitative assessment of sea ice concentrations and thicknesses.

Nonetheless, we consider this direct (and first) intercomparison of proxy- and model-based sea ice estimates an encouraging attempt that provides a new perspective on the use of a PIP_{25} index as quantitative means for sea ice reconstructions.

5. Conclusions

With the consideration of the sea ice proxy IP_{25} and biomarkers derived from open-water phytoplankton (i.e., brassicasterol, dinosterol, and short-chain *n*-alkanes) we gain useful information about the occurrence, the spatial and lateral extent, and the environmental impact of sea ice (e.g. where primary productivity is either stimulated or lowered due to the ice cover) in the northern North Atlantic. The coupling of IP_{25} with phytoplankton biomarkers such as brassicasterol (P_BIP_{25} index) proves to be a viable approach to determine (spring/summer) sea ice conditions as is demonstrated by the good alignment of the P_BIP_{25}-based estimate of the recent sea ice coverage with satellite observations. Modern sea ice concentrations as derived from the high-resolution ocean–sea ice model are in good agreement with the satellite data as well.

The capability of the IP_{25} proxy (in combination with a phytoplankton marker) on the one hand and the NAOSIM model on the other hand to satisfactorily trace and reproduce sea ice conditions encourages a cross-evaluation of both approaches. As we observe good correlations between P_BIP_{25} values and model data, the establishment of a proxy-model calibration (in terms of transfer functions) appears feasible. More extensive IP_{25} data, however, are a needed prerequisite to verify this approach towards a quantitative sea ice assessment. Putting IP_{25} on the agenda of further biomarker studies hence will provide for a valuable database and support model experiments to describe past and, probably even more demanded, also future sea ice variations in the Arctic realm.

Supplementary materials related to this article can be found online at doi:10.1016/j.epsl.2011.04.011.

Acknowledgements

Kai Mangelsdorf and Cornelia Karger (GFZ-Potsdam, Germany) are kindly acknowledged for auxiliary GC–MS analyses. Special thanks go to Silvio Engelmann (TU-Berlin, Germany) for help on GIS-data processing and to Frank Kauker and Michael Karcher (AWI-Bremerhaven, Germany) for support in the set up of NAOSIM. Financial support was provided by the Deutsche Forschungsgemeinschaft, through SPP INTERDYNAMIK (STE 412/24-1, LO 895/13-1 and PR 1050/3-1). We also thank the anonymous reviewers for their constructive comments on the manuscript.

Biomarker data are available at doi:10.1594/PANGAEA.759566.

References

Aagaard, K., Coachman, L.K., 1968. The East Greenland current north of Denmark Strait. Arctic 21 (3), 181–200.
Abelmann, A., 1992. Diatom assemblages in Arctic sea ice — indicator for ice drift pathways. Deep Sea Res. A 39 (2, Part 1), S525–S538.
Andersen, C., Koç, N., Jennings, A., Andrews, J.T., 2004. Nonuniform response of the major surface currents in the Nordic Seas to insolation forcing: implications for the Holocene climate variability. Paleoceanography 19, PA2003.
Bauerfeind, E., Leipe, T., Ramseier, R.O., 2005. Sedimentation at the permanently ice-covered Greenland continental shelf (74°57.7′N/12°58.7′W): significance of biogenic and lithogenic particles in particulate matter flux. J. Mar. Syst. 56 (1–2), 151–166.
Belt, S.T., et al., 2007. A novel chemical fossil of palaeo sea ice: IP_{25}. Org. Geochem. 38 (1), 16–27.
Belt, S.T., et al., 2010. Striking similarities in temporal changes to spring sea ice occurrence across the central Canadian Arctic Archipelago over the last 7000 years. Quat. Sci. Rev. 29 (25–26), 3489–3504.
Birgel, D., Stein, R., 2004. Northern Fram Strait and Yermak Plateau: distribution, variability and burial of organic carbon and paleoenvironmental implications. In: Stein, R., MacDonald, G.M. (Eds.), The Organic Carbon Cycle in the Arctic Ocean. Springer Verlag, New York.
Birgel, D., Stein, R., Hefter, J., 2004. Aliphatic lipids in recent sediments of the Fram Strait/Yermak Plateau (Arctic Ocean): composition, sources and transport processes. Mar. Chem. 88 (3–4), 127–160.
Blumer, M., Guillard, R.R.L., Chase, T., 1971. Hydrocarbons of marine phytoplankton. Mar. Biol. 8 (3), 183–189.
Boon, J.J., et al., 1979. Black Sea sterol — a molecular fossil for dinoflagellate blooms. Nature 277, 125–127.
Boyd, T.J., D'Asaro, E.A., 1994. Cooling of the West Spitsbergen current: wintertime observations West of Svalbard. J. Geophys. Res. 99 (C11), 22597–22618.
Carstens, J.r., Wefer, G., 1992. Recent distribution of planktonic foraminifera in the Nansen Basin, Arctic Ocean. Deep Sea Res. A 39 (2, Part 1), S507–S524.
Cavalieri, D., Parkinson, C., Gloersen, P., Zwally, H.J., 1996, updated 2008. Sea Ice Concentrations from Nimbus-7 SMMR and DMSP SSM/I Passive Microwave Data, 1979–2003. National Snow and Ice Data Center, Boulder, Colorado USA. Digital media (last accessed March 2011).
Comiso, J.C., Wadhams, P., Pedersen, L.T., Gersten, R.A., 2001. Seasonal and interannual variability of the Odden ice tongue and a study of environmental effects. J. Geophys. Res. 106, 9093–9116.
de Vernal, A., et al., 2001. Dinoflagellate cyst assemblages as tracers of sea-surface conditions in the northern North Atlantic, Arctic and sub-Arctic seas: the new 'n=677' data base and its application for quantitative palaeoceanographic reconstruction. J. Quat. Sci. 16 (7), 681–698.
Dieckmann, G.S., Hellmer, H.H., 2003. The importance of sea ice: an overview. In: Thomas, D.N., Dieckmann, G.S. (Eds.), Sea Ice. Blackwell Publishing, Oxford, pp. 1–21.
Dowdeswell, J.A., Cofaigh, C.Ó., 2002. Glacier-influenced sedimentation on high-latitude continental margins. : Special Publications. Geological Society, London. 203 pp.
Eglinton, T.I., Eglinton, G., 2008. Molecular proxies for paleoclimatology. Earth Planet. Sci. Lett. 275 (1–2), 1–16.
Eicken, H., et al., 1997. Sea-ice processes in the Laptev Sea and their importance for sediment export. Cont. Shelf Res. 17 (2), 205–233.
Eicken, H., et al., 2009. Field Techniques for Sea Ice Research. University of Alaska Press, Fairbanks. 566 pp.
Fahl, K., Nöthig, E.-M., 2007. Lithogenic and biogenic particle fluxes on the Lomonosov Ridge (central Arctic Ocean) and their relevance for sediment accumulation: vertical vs. lateral transport. Deep Sea Res. I 54 (8), 1256–1272.
Gelpi, E., Schneider, H., Mann, J., Oró, J., 1970. Hydrocarbons of geochemical significance in microscopic algae. Phytochemistry 9 (3), 603–612.
Gerdes, R.d., Karcher, M.J., Kauker, F., Schauer, U., 2003. Causes and development of repeated Arctic Ocean warming events. Geophys. Res. Lett. 30 (19), 1980.
Gloersen, P., et al., 1992. Arctic and Antarctic Sea Ice, 1978–1987: Satellite Passive-Microwave Observations and Analysis. NASA SP, 511, Washington, D.C.
Goad, L., Withers, N., 1982. Identification of 27-nor-(24R)-24-methylcholesta-5,22-dien-3β-ol and brassicasterol as the major sterols of the marine dinoflagellate Gymnodinium simplex. Lipids 17 (12), 853–858.
Gosselin, M., Levasseur, M., Wheeler, P.A., Horner, R.A., Booth, B.C., 1997. New measurements of phytoplankton and ice algal production in the Arctic Ocean. Deep Sea Res. II 44 (8), 1623–1644.

Gradinger, R., 2009. Sea-ice algae: major contributors to primary production and algal biomass in the Chukchi and Beaufort Seas during May/June 2002. Deep Sea Res. II 56 (17), 1201–1212.
Haas, C., Druckenmiller, M., 2009. Ice thickness and roughness measurements. In: Eicken, H., et al. (Ed.), Field Techniques for Sea Ice Research. University of Alaska Press, Fairbanks, pp. 49–116.
Haas, C., Hendricks, S., Doble, M., 2006. Comparison of the sea-ice thickness distribution in the Lincoln Sea and adjacent Arctic Ocean in 2004 and 2005. Ann. Glaciol. 44, 247–252.
Haugan, P.M., 1999. Structure and heat content of the West Spitsbergen current. Polar Res. 18 (2), 183–188.
Hebbeln, D., Berner, H., 1993. Surface sediment distribution in the Fram Strait. Deep Sea Res. I: Oceanogr. Res. Pap. 40 (9), 1731–1745.
Horner, R., 1985. Ecology of sea ice microalgae. In: Horner, R. (Ed.), Sea Ice Biota. CRC Press, Florida, pp. 83–103.
Hubberten, H.-W., 1995. Die Expedition ARKTIS-X/2 mit FS Polarstern 1994 (The Expedition ARKTIS-X/2 of RV Polarstern in 1994). Alfred Wegener Institute for Polar and Marine Research, Bremerhaven.
Hughes, N.E., Wilkinson, J.P., Wadhams, P., 2011. Multi-satellite sensor analysis of fast-ice development in the Norske Øer Ice Barrier, northeast Greenland. Ann. Glaciol. 52 (57), 151–168.
Jokat, W., 2004. The Expedition ARKTIS XIX/4 of the Research Vessel Polarstern in 2003 Reports of Legs 4a and 4b. Alfred Wegener Institute for Polar and Marine Research, Bremerhaven.
Justwan, A., Koç, N., 2008. A diatom based transfer function for reconstructing sea ice concentrations in the North Atlantic. Mar. Micropaleontol. 66 (3–4), 264–278.
Kanazawa, A., Yoshioka, M., Teshima, S.-I., 1971. The occurrence of brassicasterol in the diatoms, *Cyclotella nana* and *Nitzschia closterium*. Bull. Jpn. Soc. Sci. Fish. 37, 889–903.
Karcher, M.J., Gerdes, R.d., Kauker, F., K˜berle, C., 2003. Arctic warming: evolution and spreading of the 1990s warm event in the Nordic seas and the Arctic Ocean. J. Geophys. Res. 108 (C2), 3034.
Kauker, F., Gerdes, R., Karcher, M., Koeberle, C., Lieser, J.L., 2003. Variability of Arctic and North Atlantic sea ice: a combined analysis of model results and observations from 1978 to 2001. J. Geophys. Res. 108 (C6), 3182.
Kierdorf, C., 2006. Variability of organic carbon along the ice-covered polar continental margin of East Greenland, PhD thesis, University of Bremen, Bremerhaven, 241 pp.
Knies, J., 2005. Climate-induced changes in sedimentary regimes for organic matter supply on the continental shelf off northern Norway. Geochim. Cosmochim. Acta 69 (19), 4631–4647.
Knies, J., Kleiber, H.-P., Matthiessen, J., M¸ller, C., Nowaczyk, N., 2001. Marine ice-rafted debris records constrain maximum extent of Saalian and Weichselian ice-sheets along the northern Eurasian margin. Glob. Planet. Change 31 (1–4), 45–64.
Koç Karpuz, N., Schrader, H., 1990. Surface sediment diatom distribution and Holocene Paleotemperature variations in the Greenland, Iceland and Norwegian Sea. Paleoceanography 5, 557–580.
Koç, N., Jansen, E., Haflidason, H., 1993. Paleoceanographic reconstructions of surface ocean conditions in the Greenland, Iceland and Norwegian seas through the last 14 ka based on diatoms. Quat. Sci. Rev. 12 (2), 115–140.
Kohly, A., 1998. Diatom flux and species composition in the Greenland and Norwegian Sea in 1991–1992. Mar. Geol. 145, 293–312.
Krause, G., Schauer, U., 2001. The Expeditions ARKTIS XVI/1 and ARKTIS XVI/2 of the Research Vessel Polarstern in 2000. Alfred Wegener Institute for Polar and Marine Research, Bremerhaven.
Lemke, P., 2003. The Expedition ARKTIS XVIII/1a, b of the Research Vessel Polarstern in 2002. Alfred Wegener Institute for Polar and Marine Research, Bremerhaven.
Lisitzin, A.P., 2002. Sea-Ice and Iceberg Sedimentation in the Ocean: Recent and Past. Springer, Berlin Heidelberg New York.
Lorenz, S.J., Lohmann, G., 2004. Acceleration technique for Milankovitch type forcing in a coupled atmosphere–ocean circulation model: method and application for the Holocene. Clim. Dyn. 23 (7), 727–743.
Martin, T., Wadhams, P., 1999. Sea-ice flux in the East Greenland Current. Deep Sea Res. Part II: Top. Stud. Oceanogr. 46 (6–7), 1063–1082.
Massé, G., et al., 2008. Abrupt climate changes for Iceland during the last millennium: evidence from high resolution sea ice reconstructions. Earth Planet. Sci. Lett. 269, 565–569.
Matthiessen, J., et al., 2001. Distribution of calcareous, siliceous and organic-walled planktic mircofossils in surface sediments of the Nordic Seas and their relation to surface-water mass. In: Schäfer, P., Ritzrau, W., Schlüter, M., Thiede, J. (Eds.), The Northern North Atlantic: A changing environment. Springer, Berlin Heidelberg New York, pp. 105–127.
Meyers, P.A., 1997. Organic geochemical proxies of paleoceanographic, paleolimnologic, and paleoclimatic processes. Org. Geochem. 27 (5–6), 213–250.
Müller, P.J., Kirst, G., Ruhland, G., von Storch, I., Rosell-Melé, A., 1998. Calibration of the alkenone paleotemperature index U37K′ based on core-tops from the eastern South Atlantic and the global ocean (60°N–60°S). Geochim. Cosmochim. Acta 62 (10), 1757–1772.
Müller, J., Massé, G., Stein, R., Belt, S.T., 2009. Variability of sea-ice conditions in the Fram Strait over the past 30,000 years. Nat. Geosci. 2 (11), 772–776.
Nürnberg, D., et al., 1994. Sediments in Arctic sea ice: implications for entrainment, transport and release. Mar. Geol. 119 (3–4), 185–214.
Peinert, R., et al., 2001. Particle flux variability in the Polar and Atlantic biogeochemical provinces of the Nordic Seas. In: Schäfer, P., Ritzrau, W., Schlüter, M., Thiede, J. (Eds.), The Northern North Atlantic: A Changing Environment. Springer, Berlin, pp. 53–68.
Perovich, D.K., et al., 2009. Transpolar observations of the morphological properties of Arctic sea ice. J. Geophys. Res. 114.
Pflaumann, U., Duprat, J., Pujol, C., Labeyrie, L.D., 1996. SIMMAX: a modern analog technique to deduce Atlantic Sea surface temperatures from planktonic foraminifera in deep-sea sediments. Paleoceanography 11 (1), 15–35.
Pflaumann, U., et al., 2003. Glacial North Atlantic: sea-surface conditions reconstructed by GLAMAP 2000. Paleoceanography 18, 1065.
Polyak, L., et al., 2010. History of sea ice in the Arctic. Quat. Sci. Rev. 29 (15–16), 1757–1778.
Ramseier, R.O., Garrity, C., Bauerfeind, E., Peinert, R., 1999. Sea-ice impact on long-term particle flux in the Greenland Sea's Is Odden–Nordbukta region, 1985–1996. J. Geophys. Res. 104 (C3), 5329–5343.
Ramseier, R.O., Garrity, C., Martin, T., 2001. An overview of sea-ice conditions in the Greenland Sea and the relationship of oceanic sedimentation to the ice regime. In: Schäfer, P., Ritzrau, W., Schlüter, M., Thiede, J. (Eds.), The Northern North Atlantic: A Changing Environment. Springer, Berlin, pp. 19–38.
Rey, F., Noji, T.T., Miller, L.A., 2000. Seasonal phytoplankton development and new production in the central Greenland Sea. Sarsia 85 (4), 329–344.
Richardson, K., Markager, S., Buch, E., Lassen, M.F., Kristensen, A.S., 2005. Seasonal distribution of primary production, phytoplankton biomass and size distribution in the Greenland Sea. Deep Sea Res. I 52 (6), 979–999.
Roeckner, E., et al., 2006. Sensitivity of simulated climate to horizontal and vertical resolution in the ECHAM5 atmosphere model. J. Clim. 19 (16), 3771–3791.
Rudels, B., 1996. The thermohaline circulation of the Arctic Ocean and the Greenland Sea. In: Wadhams, P., Dowdeswell, J.A., Schofield, A.N. (Eds.), The Arctic And Environmental Change. Gordon and Breach, Amsterdam, pp. 87–99.
Rudels, B., et al., 2005. The interaction between waters from the Arctic Ocean and the Nordic Seas north of Fram Strait and along the East Greenland Current: results from the Arctic Ocean-02 Oden expedition. J. Mar. Syst. 55 (1–2), 1–30.
Sakshaug, E., 2004. Primary and secondary production in the Arctic Seas. In: Stein, R., Macdonald, R.W. (Eds.), The Organic Carbon Cycle in the Arctic Ocean. Springer-Verlag, Heidelberg, pp. 57–82.
Schlitzer, R., 2009. Ocean Data View. http://odv.awi.de.
Schlüter, M., Sauter, E., 2000. Biogenic silica cycle in surface sediments of the Greenland Sea. J. Mar. Syst. 23 (4), 333–342.
Smith, S.L., Smith, W.O., Codispoti, L.A., Wilson, D.L., 1985. Biological observations in the marginal ice zone of the East Greenland Sea. J. Mar. Res. 43, 693–717.
Smith Jr., W.O., Baumann, M.E.M., Wilson, D.L., Aletsee, L., 1987. Phytoplankton biomass and productivity in the marginal ice zone of the Fram Strait during summer 1984. J. Geophys. Res. 92, 6777–6786.
Spielhagen, R.F., et al., 2004. Arctic Ocean deep-sea record of northern Eurasian ice sheet history. Quat. Sci. Rev. 23 (11–13), 1455–1483.
Spreen, G., Kaleschke, L., Heygster, G., 2008. Sea ice remote sensing using AMSR-E 89-Ghz channels. J. Geophys. Res. 113, C02S03.
Steele, M., Morley, R., Ermold, W., 2001. PHC: a global ocean hydrography with a high-quality Arctic Ocean. J. Clim. 14 (9), 2079–2087.
Stein, R., 1990. Organic carbon content/sedimentation rate relationship and its paleoenvironmental significance for marine sediments. Geo Mar. Lett. 10 (1), 37–44.
Stein, R., 2008. Arctic Ocean sediments: processes, proxies, and paleoenvironment. Developments in Marine Geology, 2. Elsevier, Amsterdam. 592 pp.
Stein, R., Macdonald, R.W., 2004. The Organic Carbon Cycle in the Arctic Ocean. Springer, Berlin. 363 pp.
Steinsund, P.I., Hald, M., 1994. Recent calcium carbonate dissolution in the Barents Sea: paleoceanographic applications. Mar. Geol. 117 (1–4), 303–316.
Vare, L.L., Massé, G., Gregory, T.R., Smart, C.W., Belt, S.T., 2009. Sea ice variations in the central Canadian Arctic Archipelago during the Holocene. Quat. Sci. Rev. 28 (13–14), 1354–1366.
Vinje, T., Nordlund, N., Kvambekk, Å., 1998. Monitoring ice thickness in Fram Strait. J. Geophys. Res. 103 (C5), 10437–10449.
Volkman, J.K., 1986. A review of sterol markers for marine and terrigenous organic matter. Org. Geochem. 9 (2), 83–99.
Volkman, J.K., 2006. Lipid markers for marine organic matter. In: Volkman, J.K. (Ed.), Handbook of Environmental Chemistry. Springer-Verlag, Berlin, Heidelberg, pp. 27–70.
Volkman, J.K., Barrett, S.M., Dunstan, G.A., Jeffrey, S.W., 1993. Geochemical significance of the occurrence of dinosterol and other 4-methyl sterols in a marine diatom. Org. Geochem. 20 (1), 7–15.
Volkman, J.K., et al., 1998. Microalgal biomarkers: a review of recent research developments. Org. Geochem. 29 (5–7), 1163–1179.
Wadhams, P., 1990. Evidence for thinning of the Arctic ice cover north of Greenland. Nature 345 (6278), 795–797.
Wadhams, P., 1992. Sea ice thickness distribution in the Greenland Sea and Eurasian basin, May 1987. J. Geophys. Res. 97 (C4), 5331–5348.
Wadhams, P., 1997. Ice thickness in the Arctic Ocean: the statistical reliability of experimental data. J. Geophys. Res. 102 (C13), 27951–27959.
Wadhams, P., et al., 1996. The development of the Odden ice tongue in the Greenland Sea during winter 1993 from remote sensing and field observations. J. Geophys. Res. 101, 213–235.
Wassmann, P., et al., 2004. Particulate organic carbon flux to the Arctic Ocean sea floor. In: Stein, R., Macdonald, R.W. (Eds.), The Organic Carbon Cycle in the Arctic Ocean. Springer, Berlin Heidelberg, pp. 101–138.
Wiktor, J., 1999. Early spring microplankton development under fast ice covered fjords of Svalbard. Arct. Oceanologia 41 (1), 51–72.
Zonneveld, K.A.F., et al., 2010. Selective preservation of organic matter in marine environments; processes and impact on the sedimentary record. Biogeosciences 7 (2), 483–511.